Inorganic Chemistry
Article

Inorg. Chem. **2010**, *49*, 9343–9349 **9343**
DOI: 10.1021/ic100990a

Synthesis, Crystal Structure, Atomic Hirshfeld Surfaces, and Physical Properties of Hexagonal $CeMnNi_4$

Iben Skovsen,[†] Mogens Christensen,[†] Henrik Fanø Clausen,[†] Jacob Overgaard,[†] Christian Stiewe,[‡] Titas Desgupta,[‡] Eckhard Mueller,[‡] Mark A. Spackman,[§] and Bo B. Iversen*[,†]

[†]*Centre for Materials Crystallography, Department of Chemistry and iNANO, Aarhus University, DK-8000 Århus C, Denmark,* [‡]*German Aerospace Center (DLR), Linder Hoehe, DE-51147 Cologne, Germany, and* [§]*School of Biomedical, Biomolecular & Chemical Sciences, University of Western Australia, Crawley, WA 6009, Australia*

Received May 18, 2010

The hexagonal polymorph of $CeMnNi_4$ has been synthesized using cold crucible, high-frequency induction melting with subsequent Czochralski crystal pulling. Single-crystal X-ray diffraction, multitemperature synchrotron powder X-ray diffraction (90 to 600 K), and neutron powder diffraction data have been measured to establish the detailed crystal structure and in particular the location of the Mn atoms. The neutron diffraction data provide sufficient scattering contrast between Mn and Ni to establish that the 2*c* site has an occupancy of 13% Mn atoms, while the 3*g* site has an occupancy of 25% Mn atoms. Thus, the crystal structure is complex with considerable disorder. Rietveld refinement of the multitemperature synchrotron data establishes a near linear thermal expansion coefficient of $13.9(3) \times 10^{-6}\ K^{-1}$ and $14.9(3) \times 10^{-6}\ K^{-1}$ for the *a* and *c* axes, respectively. Atomic Hirshfeld surfaces are introduced as a new tool to investigate the atomic coordination and interactions in intermetallic compounds. The atomic displacement parameters (ADPs) are observed to be much larger for the heavy Ce atom than for the lighter Mn and Ni atoms, and this correlates with the large atomic Hirshfeld volume of Ce relative to Mn and Ni. The fit of a Debye model to the ADPs gives θ_D = 312(3) K. Magnetic susceptibility data measured between 2 and 350 K indicate ferromagnetic ordering at 122(2) K (Weiss constant) based on a linear fit of the inverse magnetic susceptibility in the paramagnetic region. Transport properties were measured on a polycrystalline sample containing CeO_2 (2.8%) and Ni (7.7%) impurities. The electrical conductivity is observed to be metallic with a distinct kink in the data around 120 K coinciding with the observed Curie temperature. The lattice thermal conductivity (κ_L) increases from 0.5 W/Km at 2 K to 8 W/Km at 50 K, and the relatively moderate value of κ_L probably reflects the significant structural disorder.

Introduction

The compound $CeMnNi_4$ has received attention due to potential applications in spintronics.[1−6] Two different polymorphs with the stoichiometry $CeMnNi_4$ exist, and the most investigated compound is the cubic phase belonging to the space group $F\bar{4}3m$.[2] The hexagonal polymorph belonging to space group *P*6/*mmm* has been much less studied. The cubic phase has distinct locations of the Mn and Ni atom in the crystal structure, where the Mn atoms are located in large voids. Correspondingly, the Mn atoms have large thermal motion, which is reminiscent of rattling atoms in thermoelectric clathrates and skutterudites.[7−10]

The hexagonal phase is isostructural to $CeNi_5$,[11] but when Ni is replaced with Mn to form $CeMnNi_4$, there is no obvious site for the Mn atoms to occupy. The weak X-ray scattering contrast between Mn and Ni makes it difficult to determine the specific location of Mn atoms using conventional X-ray diffraction. Figure 1 shows the $CeNi_5$ structure, where turquoise Ce is at the origin (0, 0, 0) and Ni atoms occupy both the red 2*c* (2/3, 1/3, 0) and the yellow 3*g* (1/2, 0, 1/2) sites.

*To whom correspondence should be addressed. E-mail: bo@chem.au.dk.

(1) Mazin, I. I. *Phys. Rev. B* **2006**, *73*, 012415.
(2) Dhiman, I.; Das, A.; Dhar, S. K.; Raychaudhuri, P.; Singh, S.; Manfrinetti, P. *Solid State Commun.* **2007**, *141*, 160.
(3) Klimczak, M.; Talik, E.; Kusz, J.; Kowalchyk, A.; Tolinski, T. *Cryst. Res. Technol.* **2007**, *42*, 1348.
(4) Murugan, P.; Singh, A. K.; Das, G. P.; Kawazoe, Y. *Appl. Phys. Lett.* **2006**, *89*, 222502.
(5) Voloshina, E. N.; Dedkov, Y. S.; Richter, M.; Zahn, P. *Phys. Rev. B* **2006**, *73*, 144412.
(6) Singh, S.; Sheet, G.; Raychaudhuri, P.; Dhar, S. K. *Appl. Phys. Lett.* **2006**, *88*, 022506.
(7) Nolas, G. S.; Slack, G. A. *Am. Sci.* **2001**, *89*, 136.
(8) Iversen, B. B.; Palmquist, A. E. C.; Cox, D. E.; Nolas, G. S.; Stucky, G. D.; Blake, N. P.; Metiu, H. *J. Solid State Chem.* **2000**, *149*, 455.
(9) Nolas, G. S.; Morelli, D. T.; Tritt, T. M. *Annu. Rev. Mater. Sci.* **1999**, *29*, 89.
(10) Sales, B. C.; Mandrus, D.; Chakoumakos, B. C.; Keppens, V.; Thomson, J. R. *Phys. Rev. B* **1997**, *56*, 15081.
(11) Murugan, P.; Bahramy, M. S.; Kawazoe, Y. *Phys. Rev. B* **2008**, *77*, 064401.

Published on Web 09/16/2010

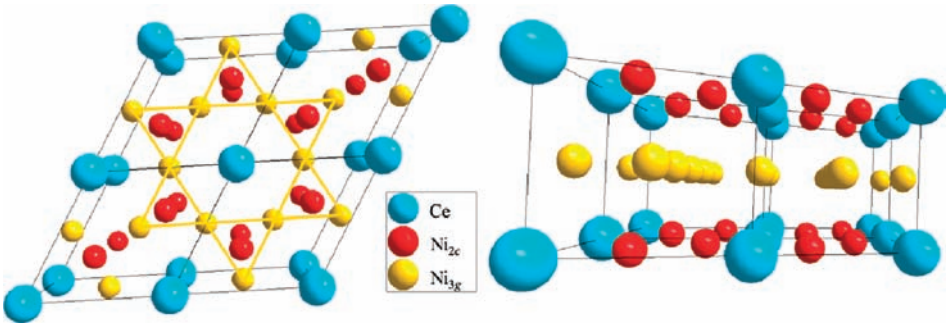

Figure 1. The structure of hexagonal $CeNi_5$, with turquoise balls representing Ce, red balls representing Ni on the 2*c* site, and yellow balls representing Ni on the 3*g* site. The kagomé lattice has been indicated with yellow triangles. The view on the right shows that the kagomé lattice is present in distinct layers in the structure.

It has been stated that more space appears to be available around the 3*g* site than around the 2*c* site, and keeping the cubic structure in mind, it is therefore expected that Mn prefers the 3*g* sites over the smaller 2*c* sites.[11] Below, we introduce atomic Hirshfeld surfaces as a new tool to provide more rigorous structural analysis of the atomic volumes.

The substitution of Ni by Mn has the interesting consequence that $CeNi_5$ changes from being a Pauli paramagnet to becoming a ferromagnet with phase transition at 135 K.[12,13] However, this was shown for a compound with stoichiometry $CeMn_{0.75}Ni_{4.25}$, and no information is available for $CeMnNi_4$. The atoms in the 3*g* layers actually form a kagomé lattice (see Figure 1),[11] and the magnetic structure is possibly susceptible to small changes of the magnetic ions. Indeed, other $CeXNi_4$ (X = Sc−Co, B, Al, etc.) compounds have been investigated magnetically, and a large variety of properties are displayed. Hexagonal $CeMnNi_4$ is shown here to be ferromagnetic just as cubic $CeMnNi_4$,[2] and the cubic structure $CeFeNi_4$.[14] First principles theoretical studies suggest that the hexagonal series $CeScNi_4$ to $CeCoNi_4$ is ferromagnetic.[11] That study also predicted $CeCrNi_4$ to be antiferromagnetic. $CeCuNi_4$, $CeAlNi_4$, and $CeBNi_4$ have been shown experimentally to be paramagnetic.[15,16] Finally, theoretical studies have indicated that $CeTiNi_4$ and $CeVNi_4$ are diamagnetic.[11]

In this paper, we investigate structural and physical properties of hexagonal $CeMnNi_4$. Neutron powder diffraction and single-crystal X-ray diffraction were used to clarify the occupancy of Mn and Ni in the structure, while multitemperature synchrotron powder diffraction was used to follow structural changes as a function of temperature. Atomic Hirshfeld surface analysis is introduced to understand the coordination and chemical interactions in this intermetallic compound. Finally, the magnetic susceptibility was measured between 2 and 350 K and the transport properties between 2 and 950 K.

Experimental Section

Synthesis. The hexagonal polymorph of $CeMnNi_4$ was prepared by melting stoichiometric amounts of the elemental constituents (99.9 wt % purity Ce and Mn, 99.99 wt % purity Ni). The stoichiometric pure elements were placed in a water-cooled copper hearth and heated by high-frequency induction. The sample was remelted four times, and prior to melting the sample was cleaned in 2 M nictric acid and flipped to ensure homogenization. Subsequently, an ingot was pulled from the melt using the Czochralski method. A molybdenum wire was used instead of a seed crystal, and the resulting ingot (mass = 8.7 g) is shown in Figure 2.

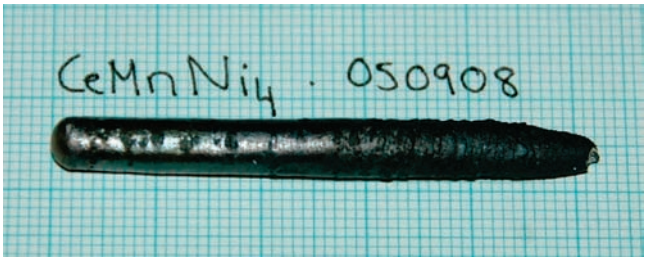

Figure 2. Photo of the as-synthesized sample after Czochralski pulling. The squares on the paper are 1 × 1 mm.

Synchrotron Powder X-Ray Diffraction. Part of the Czochralski pulled sample was ground and investigated by multitemperature, high-resolution synchrotron powder X-ray diffraction (PXRD). The PXRD data were collected at beamline BL02B2, SPring8, Japan, using a large Debye−Scherrer camera.[17] A homogeneous grain size is important for measuring high-quality PXRD data. The powders were first floated with ethanol in a Petri dish and left for sedimentation. The top layer of the ethanol was transferred to a new Petri dish and left for further sedimentation. The top layer was removed again and placed into a new Petri dish, and the ethanol was evaporated, leaving a sample fraction of homogeneous grain size. The sample was transferred to a 0.2 mm quartz capillary and held in an ultrasound bath to obtain a dense packing of the powder. The synchrotron radiation wavelength was determined to be $\lambda = 0.357469(8)$ Å using a CeO_2 standard ($a = 5.411102$ Å). Temperature control for data collected below room temperature (90−300 K) was obtained with a nitrogen flow system, while data at elevated temperatures (300−600 K) were collected using a separate hot nitrogen flow system. All data were Rietveld-refined using the program FULLPROF.[18] Data above $2\theta = 61°$ were found to be very weak for all measurements and were consequently omitted in the final refinements.

Single Crystal X-Ray Diffraction. A single crystal with approximate dimensions of $50 \times 80 \times 60\ \mu m^3$ was glued to the end

(12) Nordström, L.; Brooks, M. S. S.; Johansson, B. *Phys. Rev. B* **1992**, *46*, 3458.
(13) Pourarian, F.; Liu, M. Z.; Lu, B. Z.; Huang, M. Q.; Wallace, W. E. *J. Solid State Chem.* **1986**, *65*, 111.
(14) Pourarian, F.; Pedziwiatr, A.; Wallace, W. E. *J. Appl. Phys.* **1984**, *55*, 1981.
(15) Kowalczyk, A.; Tolinski, T.; Andrzewski, B.; Szlaferek, A. *J. Alloys Compd.* **2006**, *413*, 1.
(16) Tolinski, T.; Kowalchyk, A.; Chelkowska, G.; Pugaczowa-Michalska, M.; Andrzejewski, B.; Ivanov, V.; Szewczyk, A.; Gutowska, M. *Phys. Rev. B* **2004**, *70*, 064413.
(17) Nishibori, E.; Takata, M.; Kato, K.; Sakata, M.; Kubota, Y.; Aoyagi, S.; Kuroiwa, Y.; Yamakata, M.; Ikeda, N. *J. Phys. Chem. Solids* **2001**, *62*, 2095.
(18) Rodriguez-Carvajal, J. In *FULLPROF*, V. 2009 (March); Laboratoire Leon Brillouin (CEA-CNRS): France, 1997.

of a glass fiber. Single crystal diffraction data were collected on an APEX-II Bruker diffractometer equipped with a Mo Kα source at Aarhus University. The sample was kept at 100 K using an Oxford nitrogen cryostream. The collected data were indexed with the hexagonal space group and integrated using SAINT+. The data were absorption corrected using SADABS and subsequently refined using SHELX.[19] The structural model allowed refinement of the Ni/Mn occupancies on both the 2*c* and the 3*g* site. However, to overcome large parameter correlations, each of the sites were constrained to be fully occupied, and the total sum of Mn was constrained to be one atom/unit cell.

Neutron Powder Diffraction. The sample for the neutron powder diffraction experiment was prepared as described above but without the final Czochralski pulling. This presumably is the reason why no Ni and CeO_2 impurities were detected in this sample. The prepared sample of mass 6.7 g was loaded into a vanadium container with a diameter of 4 mm. The neutron powder diffraction pattern was collected at room temperature using the banana-shaped detector of Echidna at ANSTO, Australia.[20] The neutron wavelength was $\lambda = 1.6225(1)$ Å, obtained by calibration with an Al_2O_3 standard. The powder diffraction pattern was refined using FULLPROF.[18]

Energy Dispersive X-Ray Spectroscopy (EDX). The overall stoichiometry of the Czochralski pulled sample was determined by energy dispersive X-ray spectroscopy (EDX). The sample was placed in a CamScan Maxim electron microscope. An acceleration voltage of 20 kV was used to emit characteristic X-rays. The emitted X-rays were detected with a liquid-nitrogen-cooled solid-state detector. The obtained spectrum was chosen to contain the K edges of Mn and Ni, while the L edge was used for the detection of Ce.

Physical Properties. Transport properties in the range from 2 to 300 K were measured using a Quantum Design physical properties measurement system (PPMS) equipped with the thermal transport option (TTO) at Aarhus University. The TTO employs a four-point contact technique, and quasi-static conditions are used for simultaneous measurements of the Seebeck coefficient and electric and thermal conductivity. A sample of dimensions $5\times5\times14$ mm^3 was cut from the bulk sample produced before Czochralski pulling, and visible cracks were avoided. Several attempts of synthesizing a single crystal large enough for physical property measurements were unsuccessful, and the polycrystalline sample containing an impurity of cubic $CeMnNi_4$ was therefore used.

Transport properties above room temperature were measured at the German Aerospace Center using a home-built four-point probe for the electrical conductivity measurement and a combination of LFA (laser flash apparatus) and a DSC (differential scanning calorimetry) for the thermal conductivity measurement. The thermal conductivity in the high-temperature range was determined from the thermal diffusivity (using a Netzsch LFA 427) and the heat capacity (using a Netzsch DSC 404). Pellets of dimensions 13.65 mm diameter and 1.85 mm thickness were prepared for characterization.

The magnetic susceptibility was measured using the ACMS option in the PPMS. A piece of the Czochralski pulled ingot was mounted in a straw and measured in the temperature range from 2 to 350 K in a field of 0.20 T.

Results and Discussion

Crystal Structure. The starting model for the neutron powder diffraction data was the $CeNi_5$ structure, but Mn atoms were then introduced on both the 2*c* and the 3*g* sites.

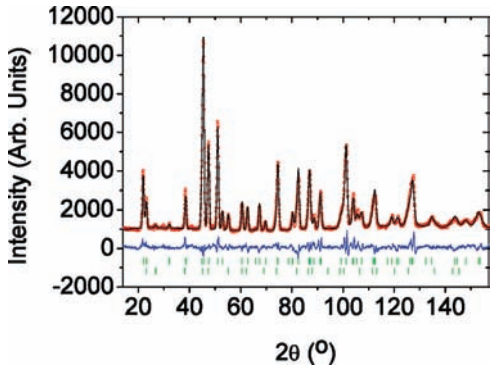

Figure 3. Observed (red circles), calculated (black line), and difference (blue line) intensity for the Rietveld refinement of neutron powder diffraction data for hexagonal $CeMnNi_4$. The green markers indicate positions of Bragg peaks for hexagonal $CeMnNi_4$ (top) and cubic $CeMnNi_4$ (bottom).

Table 1. Crystallographic Details for the Neutron Powder Diffraction and Single Crystal X-Ray Diffraction Data

	powder neutron	single crystal X-ray
temp/K	300	100
exposure time	4 h	N/A
N(obs)/N(ref)	2810	4040
N(ref)/N(unique ref)	81	223
N(par)	32	11
$R_F/R_{all}(F)$	0.0390	0.0148
$R_{Bragg}/R_{4\sigma}(F)$	0.0676	0.0136
$R_p/wR_{all}(F^2)$	0.150	0.0336
$R_{wp}/wR_{4\sigma}(F^2)$	0.151	0.0333
χ^2/GoF	6.581	1.213
a/Å	4.9171(1)	4.9178(2)
c/Å	4.0273(1)	4.0394(2)
sof(Ni_{2c})	87(1)%	89(1)%
sof(Ni_{3g})	75(1)%	74(1)%

The Mn and Ni occupancies were allowed to refine freely. The ADPs of the Ni and Mn atoms were constrained to an identical value on each site, and both the 2*c* and 3*g* sites were constrained to be fully occupied. The neutron scattering contrast between Ni and Mn is large, as the neutron scattering lengths are 10.3 and −3.73 fm, respectively. Figure 3 shows the observed and calculated data obtained from Rietveld refinement of the powder neutron diffraction data.

Unlike the X-ray data modeled below, the neutron data do not contain intensity from metallic Ni or CeO_2; however a significant amount of cubic $CeMnNi_4$ is found. The sample used for neutron X-ray diffraction was taken from another batch than samples used for all other studies presented in this paper. Selected details from the Rietveld refinement and the single crystal X-ray diffraction are listed in Table 1. Full details of the refinement are found in the Supporting Information.

The results obtained from single-crystal X-ray and neutron powder diffraction agree well. EDX spectra were recorded eight different places on the *as-synthesized* polycrystalline bar, and the average composition was determined to be 17.3(9) atom % Ce, 12.1(6) atom % Mn, and 71(4) atom Ni. This gives an average composition of $CeMn_{0.7}Ni_{4.1}$, which is slightly lower in Mn concentration than refined from the diffraction data. However, the EDX data average over the entire sample, including the impurities, whereas the diffraction data only determine the content in the specific crystal structure.

(19) Sheldrick, G. M. *SADABS*; *SHELX*; Bruker AXS Inc.: Madison, WI, 2003.
(20) Liss, K.-D.; Hunter, B.; Hagen, M.; Noakes, T.; Kennedy, S. *Physica B* **2006**, *385*−*386*, 1010.

$CeMnNi_4$ has been studied by Murugan et al. using first-principles density functional theory calculations.[11] It was concluded that for the series of compounds $CeXNi_4$ (X = Sc−Co), the substitutional M atom would prefer the presumed larger 3*g* site rather than the smaller 2*c* site. Consequently, the derived structure reduces to an orthorhombic structure with the space group *Cmmm*.[4,11] The neutron powder and single-crystal X-ray results are in agreement with the expectation that a larger amount of Mn is found on the 3*g* site compared with 2*c*. Nevertheless, it is clear that the 2*c* site does hold a significant fraction of the total amount of manganese (~25%) present in the structure. This gives a more complex crystal structure than suggested in studies of $LnXNi_4$ structures and considered theoretically.

The isostructural compounds LaT_xNi_{5-x} (T = Fe, Mn) have been investigated by Yang et al.[21] Neutron diffraction data on $LMnNi_4$ revealed that 86% of the manganese was located at the 3*g* site.[22] For $LaFeNi_4$, Mössbauer studies indicate that the 3*g* site has 95% Fe.[23] The present results show that the 3*g* site only has about 75% Mn atoms in the case of $CeMnNi_4$. Thus, the different structures do not have the same occupancies of X and Ni, and comparison of physical properties such as magnetism is not straightforward.

Atomic Hirshfeld Surfaces. Atomic interactions in intermetallic compounds are not easily understood due to the many bonding possibilities. In order to gain insight into these interactions and the site preference of Mn in the structure, the partitioning scheme of Hirshfeld surfaces implemented in CrystalExplorer has been utilized.[24] The Hirshfeld surface uses the stockholder concept to divide the electron density of a molecule into atomic fragments.[25] The concept was generalized to extract molecular fragments from a crystal by defining a molecular weight function, $w(\mathbf{r}) = \rho_{\text{promolecule}}(\mathbf{r})/\rho_{\text{procrystal}}(\mathbf{r})$. The promolecule density is a sum of spherically averaged atomic electron density functions centered on the atomic positions for the selected molecular fragment, whereas the procrystal density is the corresponding density of the surrounding crystal.[26] Spackman and co-workers suggested a partitioning of space into regions where the promolecule density dominates, e.g., $w(\mathbf{r}) \geq 0.5$, as a unique new scheme defining a so-called Hirshfeld surface.[27,28]

In intermetallic compounds, there are typically no well-defined "molecular fragments", and we therefore introduce atomic Hirshfeld surfaces defined as the region where the particular atomic density dominates. This novel approach provides a way of identifying plausible bonding patterns in nonmolecular crystal structures, as well as providing a quick tool for analyzing the atomic environments. One property that can reveal interesting details about the atomic environments is the curvedness of the Hirshfeld surface as defined by McKinnon et al.[28]

Table 2. Volumes (Å^3) of the Hirshfeld Atoms in the Two $CeNi_5$ Structures

	$CeNi_5$, this study	$CeNi_5$, literature
V(Ce)	15.0	15.0
$V(Ni_{2c})$	7.5	7.4
$V(Ni_{3g})$	7.6	7.5

The volumes of the Hirshfeld atoms have been calculated for Ce, Ni_{2c}, and Ni_{3g} for two different structures, and they are listed in Table 2. First, a $CeNi_5$ structure has been generated by using the fractional coordinates from the present $CeMnNi_4$ structure with both the 2*c* and 3*g* site fully occupied by nickel. Second, the $CeNi_5$ structure obtained from the literature was included as a reference material.[29] Cell parameters for the reference material are 4.860 Å and 3.996 Å for *a* and *c*, respectively, obtained by X-ray diffraction, and they are similar to values obtained by synchrotron X-ray diffraction in this study (although *c* differs slightly). Hence, we would expect that the Hirshfeld analysis of both structures would give similar results.

The atomic Hirshfeld volumes of the two structures are virtually identical. Interestingly, the two crystallographically distinct Ni sites have very similar Hirshfeld volumes, in contradiction with the idea that the 3*g* site should be slightly larger than the 2*c* site.[11,22,30] Solely on the basis of the atomic sizes of Mn and Ni (atomic radii of 140 and 135 pm, respectively), the Hirshfeld analysis does not predict a site preference for Mn atoms in the hexagonal $CeNi_5$ structure. This agrees well with the experimental data described above, which showed that Mn substitutes on both sites. This corroborates that the site preference of Mn in this structure is not correlated directly to the size of the crystallographic sites.

In intermetallic compounds, it is often very difficult to assign bonding interactions and assign the precise coordination of the atoms. It would therefore be an important step in understanding the properties of intermetallic systems if there was a straightforward tool available to recognize the atomic interactions. The curvedness mapped on the Hirshfeld surfaces of Ce, Ni_{2c}, and Ni_{3g} is shown in Figure 4 obtained from the structure with Mn fully substituted by Ni.

The curvedness varies from blue (large curvature) to red (flat), where the latter identifies flat regions that reflect closer contacts between adjacent atoms. As these regions are likely to indicate directional atom−atom interactions, we draw a parallel between the curvedness of the Hirshfeld surface and possible directional atom−atom interactions in intermetallic systems such as these. In this manner, this can provide information about the coordination number of an atom, which is easily recognized in the pattern of curvedness on the Hirshfeld surface. Furthermore, the closer the contact, the more deformed (flattened) the atomic Hirshfeld surface will be, and this may be correlated to the strength of the intermetallic interaction.

(21) Yang, J. B.; Tai, C. Y.; Marasinghe, G. K.; Waddill, G. D.; Pringle, O. A.; James, W. J.; Kong, Y. *Phys. Rev. B* **2000**, *63*, 014407.
(22) (a) Lartigue, C.; Percheron-Guégan, A.; Achard, J. C. *J. Less-Common Metals* **1980**, *75*, 23. (b) Lartigue, C.; Percheron-Guegan, A.; Achard, J. C.; Tasset, F. *Rare Earth Res. Conf. 2* **1980**, 585.
(23) Lamloumi, J.; Percheron-Guégan, A.; Arcard, J. C.; Jehanno, G.; Givord, D. *J. Phys.* (*Paris*) **1984**, *45*, 1643.
(24) Wolff, S. K.; Grimwood, D. J.; McKinnon, J. J.; Jayatilaka, D.; Spackman, M. A. In *Crystal Explorer*, V. 2.0.0 alpha (r367); University of Western Australia: Crawley, Australia, 2007.
(25) Hirshfeld, F. L. *Theor. Chim. Acta* **1977**, *44*, 129.
(26) Clementi, E.; Roetti, C. *At. Data Nucl. Data Tables* **1974**, *14*, 177.
(27) Spackman, M. A.; Byrom, P. G. *Chem. Phys. Lett.* **1997**, *267*, 215.
(28) McKinnon, J. J.; Spackman, M. A.; Mitchell, A. S. *Acta Crystallogr.* **2004**, *B60*, 627.
(29) Pourarian, F.; Wallace, W. E. *J. Less-Common Metals* **1982**, *87*, 275.
(30) Flandorfer, H.; Rogl, P.; Hiebl, K.; Bauer, E.; Lindbaum, A.; Gratz, E.; Godart, C.; Gignoux, D.; Schmitt, D. *Phys. Rev. B* **1994**, *50*, 15527.

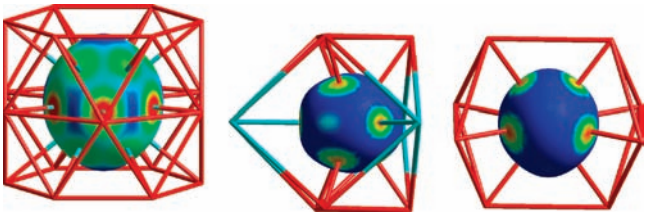

Figure 4. Curvedness plotted on the atomic Hirshfeld surfaces of Ce, Ni_{2c}, and Ni_{3g} mapped from −1 (flat; red) to −0.5 (sphere-like; blue). The two nickel positions (2*c* and 3*g*) are, in these figures, both red, and the cerium site is turquoise.

Table 3. "Strength" and Interatomic Distances for Interactions between the Atoms Ce, 2*c*, and 3*g* and Their Neighbours, with s Indicating Strong Interactions; m, Medium Strength Interactions; and w, Weak Interactions

	neighbor			
atom	Ce	(2*c*)	(3*g*)	total
Ce	0	6 (s)	12 (m)	6 (s) + 12 (m)
interatomic distances		2.807 Å	3.152 Å	
(2*c*)	3 (s)	3 (w)	6 (s)	9 (s) + 3 (w)
interatomic distances	2.807 Å	2.807 Å	2.449 Å	
(3*g*)	4 (w)	4 (s)	4 (s)	8 (s) + 4 (w)
interatomic distances	3.152 Å	2.449 Å	2.431 Å	

The coordination numbers of Ce and the two Ni sites in the $CeNi_5$ structure have been estimated on the basis of regions of the atomic Hirshfeld surface having low curvedness, Table 3. The "strength" of the interactions (strong, medium, or weak) was assigned qualitatively from the curvedness. As an example, Ce has no interactions with other Ce atoms, six strong interactions with the 2*c* site, and 12 medium interactions with the 3*g* site. It is clear that the strength of the interactions does not only depend on the interatomic distances. The 2*c* site has identical interatomic distances to both neighboring Ce and 2*c*, but the strength of the two interactions is interpreted as strong and weak, respectively. This shows that prudent interpretation is necessary when comparing curvedness for different atom pairs (e.g., Ce···Ce with Ce···Ni). To go beyond the crude observations upon which Table 3 is based would require calibrating curvedness against interaction strength as a function of interatomic distance for relevant atom pairs. This is beyond the scope of the present paper.

The strong and medium interatomic interactions in the structure are shown in Figure 5. The curvedness suggests that Ce interacts more strongly with the 2*c* atoms in the layer (Figure 1) than with the 3*g* atoms of the kagomé lattice. In contrast, the 2*c* atoms in the "Ce layer" appear to interact strongly with the 3*g* layer. Interestingly, the 3*g* atoms have strong interactions with other 3*g* atoms. For the 2*c* atoms, the strong interactions are with either Ce or 3*g*. This may suggest that magnetic ordering in the structure first takes place in the 3*g* layer, which may have a direct magnetic exchange path. On the other hand, magnetic ordering involving 2*c* must also involve the 3*g* lattice and/or the Ce site. Overall, the atomic Hirshfeld surfaces are fairly regular, and they actually retain a quite spherical appearance, although the 3*g* site is distinctly more distorted than Ce and 2*c*.

Crystal Structure as a Function of Temperature. The 90 K synchrotron powder diffraction data are shown in Figure 6.

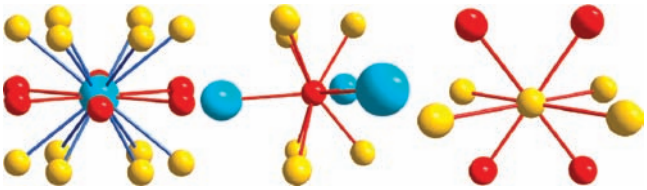

Figure 5. Coordination spheres of Ce, 2*c*, and 3*g*, respectively, only shown with strong (red bonds) and medium strength (blue bonds) interactions. For clarity, the coordination of the atoms has been shown similar to the orientation in Figure 4.

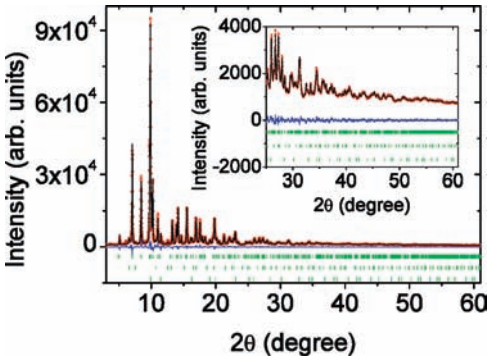

Figure 6. Observed (red), calculated (black), and difference (blue) intensity for Rietveld refinement of synchrotron powder diffraction data for hexagonal CeMnNi4. The green markers indicate positions of Bragg peaks for $CeMnNi_4$ (top), CeO_2 (middle), and nickel (bottom).

In addition to the main $CeMnNi_4$ hexagonal phase (89.6(4) wt %), there are two impurity phases CeO_2 (2.8(1) wt %) and metallic nickel (7.7(1) wt %).

Attempts were made to refine the Ni and Mn occupancies on the 2*c* and 3*g* sites, but the lacking contrast between Ni and Mn did not allow reliable refinements. Consequently, all occupancies were fixed at the values obtained from the neutron data. Selected crystallographic details are listed in Table 4 for three different temperatures (90, 300, and 600 K). Full details of the multitemperature refinements are given in the Supporting Information.

At the lowest temperature, the ADP of the 3*g* site becomes slightly negative. This may reflect that the X-ray sample has slightly higher Ni occupancy on this site than the constrained value taken from the neutron data. However, it may also be due to small uncorrected systematic errors in the data. The unit cell axes, *a* and *c*, are shown as function of temperature in Figure 7. Theoretical investigations predicted an optimized structure with $a = 4.93$ Å and a c/a ratio of 0.835.[31] These values are slightly higher (0.06−0.10 Å) than observed experimentally. The unit cell axes show near linear thermal expansion with expansion coefficients of $13.9(3) \times 10^{-6}\,K^{-1}$ and $14.9(3) \times 10^{-6}\,K^{-1}$ for *a* and *c*, respectively.

The atomic displacement parameters (ADPs) for the three different crystallographic sites are shown in Figure 8. It is clear that cerium has a larger ADP than nickel/manganese at either of the sites. This is not expected considering that Ce is a much heavier atom, but it correlates with the fact that Ce has a much larger Hirshfeld volume. Furthermore, it can be seen that Ni/Mn at the 2*c* site has

(31) Murugan, P.; Singh, A. K.; Das, G. P.; Kawazoe, Y. *Condens. Matter* [Online] arXiv:cond-mat/0510748v1, **2005**.

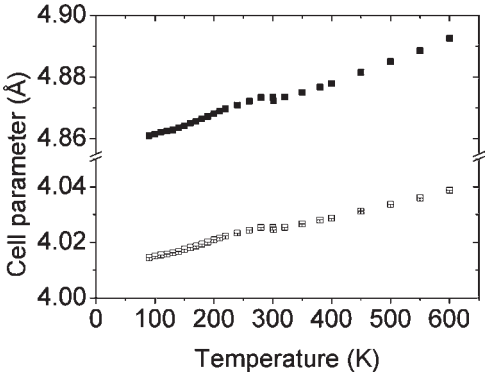

Figure 7. Lattice parameters a (■) and c (□) for hexagonal $CeMnNi_4$ as a function of temperature.

Table 4. Crystallographic Details for the Synchrotron Powder Diffraction Data

temp/K	90	300	600
exposure time/min	5	5	5
N(observations)	5799	5799	5799
N(reflections)	1270	1276	1309
N(parameter)	91	91	91
R_F	0.0169	0.0197	0.0309
R_{Bragg}	0.0361	0.0371	0.0406
R_p	0.0796	0.0852	0.0990
R_{wp}	0.102	0.105	0.099
χ^2	9.12	9.11	2.70
a/Å	4.86112(1)	4.87342(1)	4.89262(1)
c/Å	4.01452(1)	4.02536(3)	4.03875(1)
X	0.582(2)	0.574(2)	0.576(2)
Y	0.0343(2)	0.0351(2)	0.0219(2)
U_{iso} (Ce)	0.0092(3)	0.0151(3)	0.0237(4)
U_{iso} (Ni/Mn_{2c})	0.0044(2)	0.0083(3)	0.0112(3)
U_{iso} (Ni/Mn_{3g})	−0.0012(2)	0.0015(2)	0.0042(3)
wt % ($CeMnNi_4$)	90.1(4)	90.1(4)	73.5(5)
wt % (CeO_2)	2.7(1)	2.5(1)	10.3(2)
wt % (Ni)	7.2(2)	7.4(2)	16.2(4)

larger ADP than Ni/Mn at the 3g site. This trend was also observed for single-crystal X-ray diffraction data and neutron powder diffraction. Since the two Ni sites have nearly identical Hirshfeld volumes, it is not possible in general to make a direct correlation between the magnitude of the thermal vibration and the volume of the Hirshfeld atoms.

Between 450 and 550 K, the increase of the Ni/Mn ADPs levels off, but no clear changes are observed in the unit cell parameters. Between 550 and 600 K, there is a significant increase in the Ni impurity level from ∼12% to ∼16% (see Table 4 and Supporting Information). However, even from 300 K, there is a tendency toward increasing Ni impurity level with increasing temperature as the weight percentage increases from ∼8% at room temperature to ∼12% at 550 K. This indicates that the structure is not thermally stable in atmospheric air at elevated temperatures. DSC/TGA data have been measured from room temperature to 1773 K on a sample from the batch measured at Spring8 (see Supporting Information). Both curves are smooth, and there are no clear signs of thermal degradation.

Physical Properties. The inverse of the magnetic susceptibility of hexagonal $CeMnNi_4$ (plus impurities) is shown in Figure 9 as a function of temperature. A fit using the Curie−Weiss law in the paramagnetic region gives a θ_C of 122(2) K. The ferromagnetic phase was also found by theoretical calculations to be the most stable phase.[31]

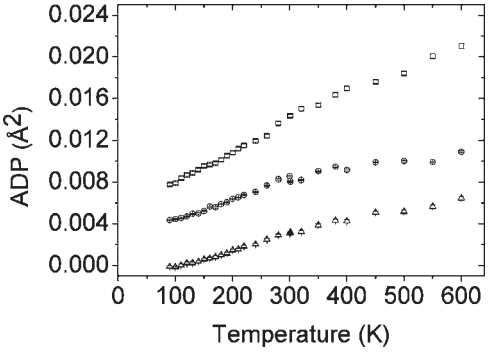

Figure 8. Atomic displacement parameters (ADPs) of Ce (□), Ni_{2c} (○), and Ni_{3g} (Δ) as a function of temperature.

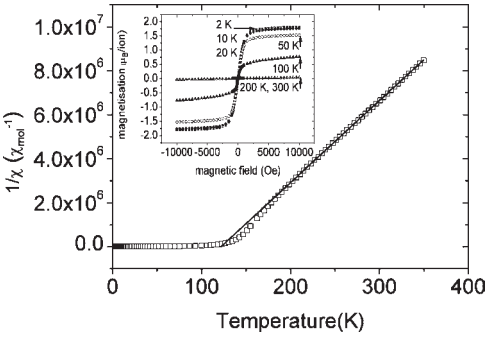

Figure 9. Inverse magnetic susceptibility as a function of temperature. The inset shows the magnetization as a function of field for 2, 10, 20, 50, 100, 200, and 300 K.

If we assume that there is one magnetic "$CeMnNi_4$ unit" per unit cell, the Curie−Weiss fit gives an effective moment of 4.1 μ_B. Since the sample was not phase-pure and it is also not clear what the electronic configurations of the individual atoms are, no specific interpretation of the origin of the moment has been attempted.

The electrical and thermal conductivities were measured between 2 and 400 K using a PPMS system, and between 700 and 950 K using a four-probe method for the electrical conductivity. The four-probe data between 300 and 700 K were faulty due to an experimental problem. The electrical resistivity is shown in Figure 10, and the material has a metallic behavior with increasing resistivity at higher temperatures. The low temperature data (2−400 K) reveal a kink in the data around 115−120 K coinciding with the observed Curie temperature. This suggests that the magnetic spin moments interact with the charge carriers. An earlier study of a single crystal of hexagonal $CeMn_{0.8}Ni_{4.2}$ reveals the same kink as observed in the present sample, and the electrical resistivity is almost identical for the two studies.[3] At high temperatures (700−950 K), the resistivity also shows a metallic behavior.

The thermal conductivity is shown in Figure 11, where low-temperature data are shown as open squares, and solid squares represent high-temperature measurements. The electronic contribution to the thermal conductivity has been estimated using Wiedemann−Franz law and subtracted from the total thermal conductivity to give the lattice thermal conductivity. The high- and the low-temperature measurements of total thermal conductivity

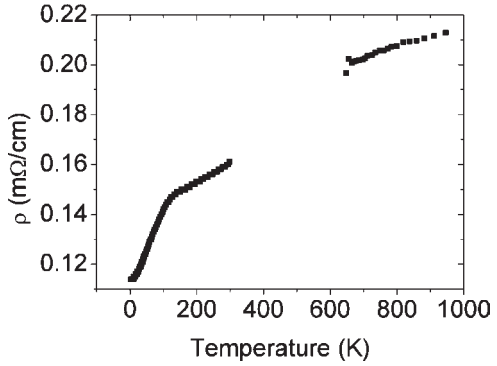

Figure 10. Electrical resistivity (ρ) as a function of temperature.

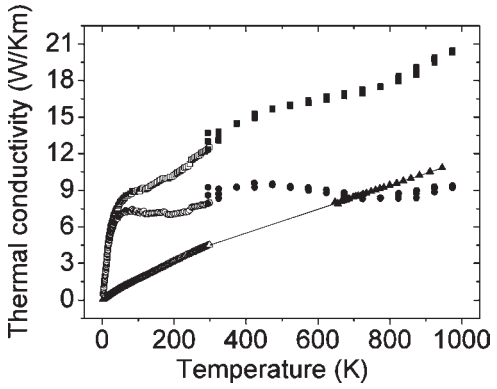

Figure 11. Thermal conductivity as a function of temperature. At low temperatures, the total thermal conductivity (open squares) is measured. The electronic conductivity (open triangles) is calculated using Wiedemann–Franz law, and the difference is assigned to lattice conductivity (open circles). At high temperatures, the symbols used are the same, although they are solid.

are in good agreement. The magnitude of the lattice thermal conductivity is relatively low for a highly crystalline compound, and the room temperature value is 8 W/Km, probably reflecting the significant atomic disorder between Mn and Ni on both the 2*c* and 3*g* sites. The electronic thermal conductivity at high temperatures (650–950 K) has been calculated as described above, and the data have been extrapolated to 300 K. The lattice thermal conductivity has been estimated by subtracting the electronic contribution from the total thermal conductivity.

Conclusions

Neutron and X-ray diffraction data have revealed and quantified a significant amount of Mn/Ni disorder in the $CeMnNi_4$ structure. This shows that typical $CeXNi_4$ structures do not have similar occupancies of X and Ni at the 2*c* and 3*g* sites, and subtle properties such as magnetism should be interpreted with care. Atomic Hirshfeld surfaces were introduced and used to establish that the 2*c* and 3*g* sites in hexagonal $CeMnNi_4$ are similar in size, and an explanation for the site preference of Mn is not established. Nevertheless, the majority of Mn is still located in the 3*g* site. The coordination environments of the atoms were examined through the curvedness of the atomic Hirshfeld surfaces. The 3*g* atoms appear to have strong interactions both with other 3*g* atoms and 2*c* atoms, whereas the 2*c* atoms have strong interactions with Ce and 3*g*. Susceptibility measurements show ferromagnetic ordering at ~122 K, and a corresponding kink is observed in the electrical resistivity data, suggesting that the magnetic spins interact with the charge carriers. A relatively low thermal conductivity of 8 W/Km was observed at room temperature, presumably reflecting the significant atomic disorder between Ni and Mn.

Acknowledgment. The work was supported by the Danish Strategic Research Council (Center for Energy Materials), the Danish Research Council for Nature and Universe (Danscatt), and The Danish National Research Foundation (Center for Materials Crystallography). The authors gratefully acknowledge the beam time obtained at the Japanese Synchrotron Radiation Facility SPring8 and the Australian Neutron Facility ANSTO and acknowledge the assistance provided by Eiji Nishibori and Avdeev Maxim during beam time.

Supporting Information Available: Crystallographic information file (CIF) for the single-crystal X-ray diffraction data, full refinement details for the neutron data, and the multitemperature synchrotron PXRD data and DSC/TGA curves. This material is available free of charge via the Internet at http://pubs.acs.org.